ELSEVIER

Journal of Nuclear Materials 313–316 (2003) 1197–1201

journal of nuclear materials

www.elsevier.com/locate/jnucmat

Radiation enhancement and impurity behavior in JT-60U reversed shear discharges

H. Kubo [a,*], S. Sakurai [a], S. Higashijima [a], H. Takenaga [a], K. Itami [a], S. Konoshima [a], T. Nakano [a], Y. Koide [a], N. Asakura [a], K. Shimizu [a], T. Fujita [a], K.W. Hill [b]

[a] *Japan Atomic Energy Research Institute, Naka-machi, Naka-gun, Ibaraki-ken 311-0193, Japan*
[b] *Princeton Plasma Physics Laboratory, P.O. Box 451, Princeton, NJ 08543, USA*

Abstract

In order to extend the high-confinement reversed shear regime with an internal transport barrier (ITB) toward high radiation loss power, Ne and Ar injection have been investigated in JT-60U. With Ne injection, high confinement ($H_{89PL} > 2.4$, $HH_{98(y,2)} > 1.6$) and high radiation loss power fraction (>80%) were simultaneously obtained at high density ($>0.7n_{GW}$). The radiation loss power was enhanced both in the main plasma and in the divertor plasma. With divertor plasma detachment and an X-point MARFE, the ITB was pronounced and the H_{89PL} factor reached 1.8. However, Ar injection resulted in excessive radiation loss enhancement inside the ITB. The Ne and the C density profile were similar to the electron density profile, and their accumulation was not significant. On the other hand, Ar showed accumulation inside the ITB.

PACS: 52.55.Fa
Keywords: Reversed shear plasma; Impurity injection; Impurity transport; JT-60U; Internal transport barrier; Radiation losses

1. Introduction

The reversed shear plasma is a promising candidate for advanced steady-state tokamak operation. Radiation loss power enhancement either in the main chamber or in the divertor is useful for mitigating the severe problem of concentrated power loading of the divertor plates, and controlled impurity injection is an effective technique for enhancing radiation while maintaining improved confinement [1–3]. In JT-60U reversed shear plasmas, compatibility between the internal transport barrier (ITB) and a detached divertor plasma has been demonstrated by radiation enhancement using Ne injection [4]. In order to extend such an operation toward high confinement, Ne and Ar have been injected into reversed shear plasmas with high confinement. However, impurity accumulation inside the ITB is a concern for reversed shear plasmas [5–8]. In this paper, radiation loss power enhancement, divertor plasma detachment and impurity behavior have been investigated in high confinement reversed shear plasmas.

2. Experiment

A quasi-steady reversed shear plasma with high confinement ($H_{89PL} \sim 3.9$, where H_{89PL} is the improvement of the energy confinement time corrected for unconfined orbit loss of fast ions compared with the ITER89-P (L-mode) scaling [9]) has recently been obtained in JT-60U [10]. For such reversed shear plasmas,

* Corresponding author. Tel.: +81-29 270 7349; fax: +81-29 270 7419.
E-mail address: kubo@naka.jaeri.go.jp (H. Kubo).

0022-3115/03/$ - see front matter
PII: S0022-3115(02)01531-3

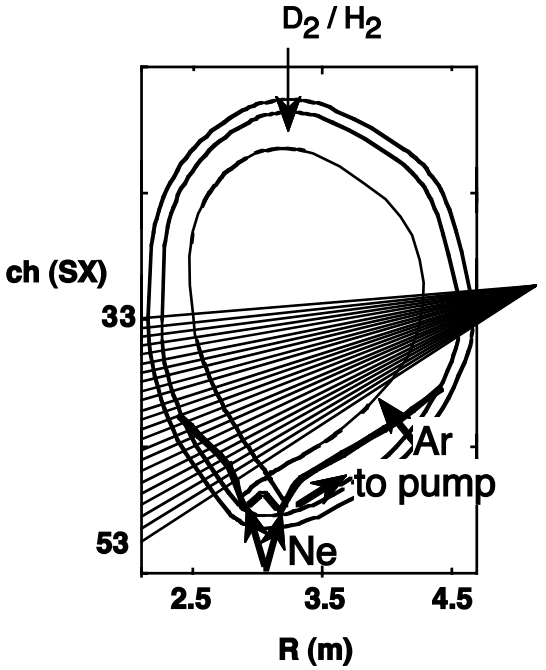

Fig. 1. Poloidal cross-section of JT-60U. The positions of gas puffing are indicated. The viewing chords of the soft X-ray emission measurement and the plasma configuration for study of Ar transport in a hydrogen discharge are shown.

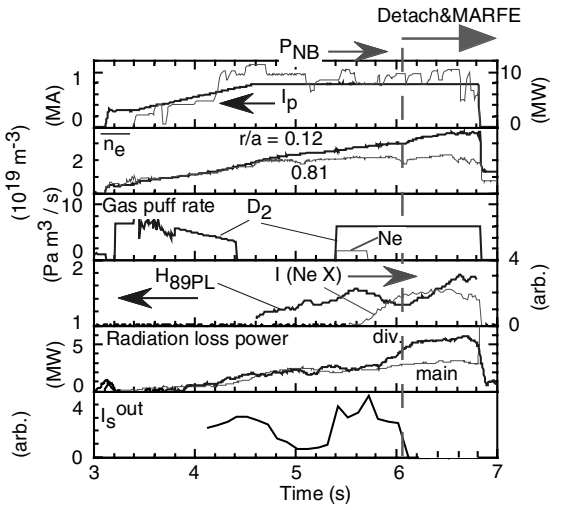

Fig. 2. Waveforms of a reversed shear plasma with Ne injection. I_p: plasma current, P_{NB}: NBI power, $\overline{n_e}$: line averaged electron densities at $r/a = 0.12$ and 0.81, gas puffing rates of D_2 and Ne, H_{89PL} factor, I(Ne X): Ne X 1.21 nm line intensity, Radiation loss power from the main and divertor plasma, I_s^{out}: ion saturation current measured with a Langmuir probe located near the outer strike point.

Ar was injected into the main chamber to enhance the radiation loss power at the edge of the main plasma [11]. In subsequent experiments, Ne was injected into the divertor to enhance the radiation loss power in the divertor plasmas, and D_2 was puffed into the main chamber from the top to control the Ne concentration by a puff-and-pump technique [12]. The positions of gas puffing are shown in Fig. 1. The major radius was ~3.3 m, the minor radius was 0.78–0.90 m, the elongation was ~1.4, the triangularity was ~0.34, the plasma current was 0.9–1.0 MA, the toroidal field was ~3.5 T, the safety factor at the 95% flux surface was 6.1–7.1, and the Greenwald density limit (n_{GW}) was $4.3–5.1 \times 10^{19}$ m^{-3}. The stored energy was controlled with a feedback technique by changing the NBI power in the range of 3–14 MW. Waveforms of a reversed shear plasma with Ne injection are shown in Fig. 2. Beginning at 4.5 s, the ITB developed, with the electron density in the core region increasing at a faster rate than that in the edge region. As shown by the H_{89PL} factor, the energy confinement improved. At 5.4 s, Ne was injected to enhance the radiation. For study of Ar transport, soft X-ray emission (the energy range was 2.7–20 keV) profiles were measured in a hydrogen discharge (the plasma current was 1.5 MA). The viewing chords of the soft X-ray emission measurement and the plasma configuration are shown in Fig. 1.

3. Results and discussion

3.1. Radiation loss power enhancement and energy confinement

The H_{89PL} factor, the ratio of the total radiation loss power (P_{rad}^{total}) to the net heating power (P_{net}) and the ratio of the radiation loss power from the main plasma (P_{rad}^{main}) to the total radiation loss power are plotted against the electron density in Fig. 3. With Ar injection, as the electron density increased from $0.6n_{GW}$ to $0.9n_{GW}$, the H_{89PL} factor decreased from 2.4 to 1.2. While P_{rad}^{total}/P_{net} stayed around 0.7, $P_{rad}^{main}/P_{rad}^{total}$ increased from 0.35 to 0.8. Then, the electron temperature at the plasma center decreased from ~6 to ~2 keV. Since some of the Ar ions were not fully ionized in this temperature range and their radiation loss efficiency was high, the radiation loss power inside the ITB increased. Moreover, accumulation of Ar (see Section 3.3) caused excessive radiation loss enhancement inside the ITB. The typical Ar density was ~2% of the electron density. With Ne injection, high confinement ($H_{89PL} > 2.4$, $HH_{98(y,2)} > 1.6$, where $HH_{98(y,2)}$ is the improvement of the thermal energy confinement time compared with the IPB98(y,2) (ELMy H-mode) scaling [13]) and high radiation loss power fraction ($P_{rad}^{total}/P_{net} > 0.8$) were simultaneously obtained at high density ($n_e > 0.7n_{GW}$). While P_{rad}^{total}/P_{net} increased, $P_{rad}^{main}/P_{rad}^{total}$ remained near 0.4. Thus, the radiation loss power from the divertor also increased. In the present

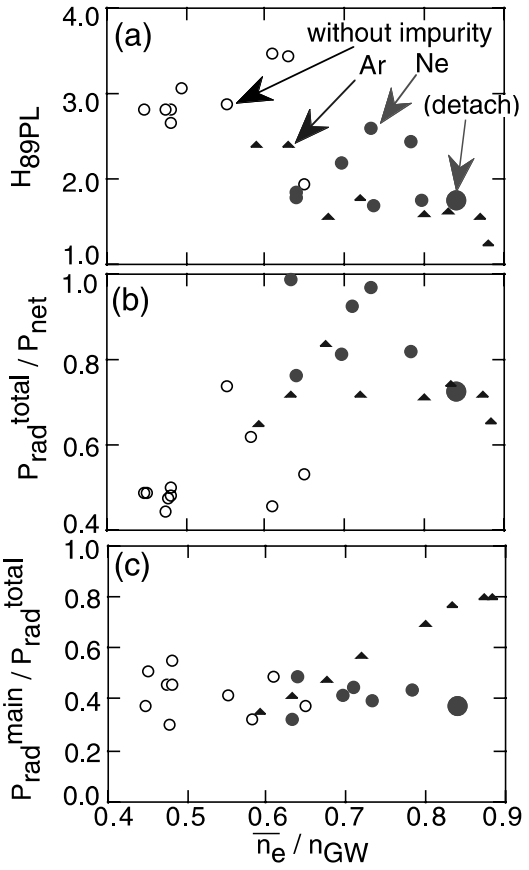

Fig. 3. (a) H_{89PL} factor, (b) ratio of the total radiation loss power to the net heating power and (c) ratio of the radiation loss power from the main plasma to the total radiation loss power against the electron density normalized by the Greenwald density limit. The large closed circles indicate a discharge with divertor plasma detachment produced by Ne injection.

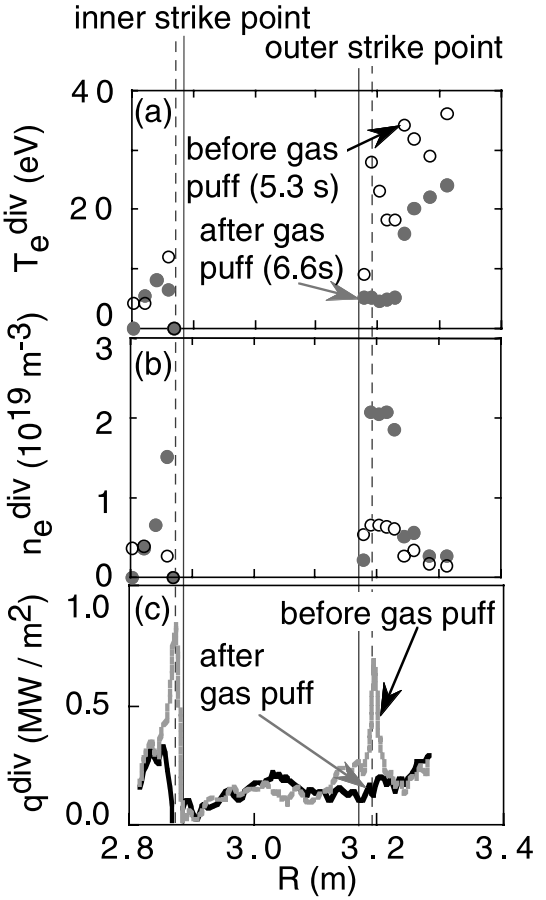

Fig. 4. Profiles of (a) the electron temperature, (b) the electron density and (c) the heat flux at the divertor plates before and after Ne puff (at 5.3 and 6.6 s) in the discharge shown in Fig. 2. The vertical lines indicate the positions of the separatrix strike points at 5.3 s (- - -) and 6.6 s (—).

study, a difference of the impurity gas puffing positions did not affect the radiation loss power distribution, since most of the injected impurity gases recycled as discussed in Section 3.3. As a result, while Ar injection resulted in excessive radiation loss enhancement inside the ITB, Ne injection was effective for obtaining a high radiation loss power fraction with high confinement at high density.

3.2. Divertor plasma detachment with Ne injection

As shown in Fig. 3, with Ne injection, the divertor plasma became detached with $H_{89PL} = 1.8$ ($HH_{98(y,2)} = 1.2$) and $P_{rad}^{total}/P_{net} = 0.73$ at $n_e = 0.84 n_{GW}$. The discharge is shown in Fig. 2. As the Ne X line intensity increased in the main plasma, the radiation loss power from the divertor increased and an X-point MARFE appeared at 6.1 s. The outer divertor plasma became detached as indicated by a decrease in the ion saturation current. With divertor plasma detachment and an X-point MARFE, the H_{89PL} factor reached 1.8. Profiles of the electron temperature, electron density and heat flux at the divertor plates before and after the Ne puff are shown in Fig. 4. The electron temperature and density were measured with Langmuir probes, and the heat flux was measured with an infrared camera. After the gas puff, a cold and dense divertor plasma was produced near the inner and outer strike points. Although the detached region was narrow (width ~ 2 cm), the maximum heat flux greatly decreased by the detachment. Radial profiles in the main plasma with divertor plasma detachment are shown in Fig. 5. The ITB is clearly seen in the profiles of the electron density, ion temperature and electron temperature. The Ne and C density were measured by charge exchange spectroscopy. The densities of Ne and C were $\sim$2.6% of the electron density. The minimum in the safety factor q_{min} was close to 3. A disruption of the discharge occurred as

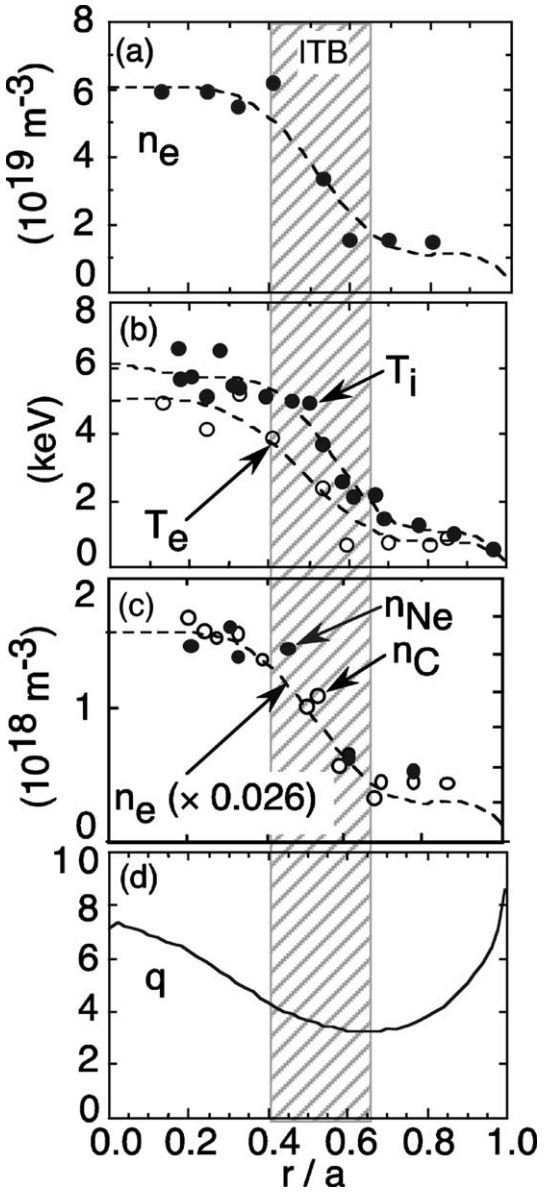

Fig. 5. Radial profiles of (a) the electron density, (b) the ion and the electron temperature, (c) the Ne, C and electron density and (d) the safety factor in the main plasma with divertor plasma detachment (at 6.6 s in the discharge shown in Fig. 2).

seen in Fig. 2, when the minimum safety factor went through $q_{\min} = 3$. Stabilization of MHD activity was needed for sustainment of the discharge.

3.3. Impurity behavior

As shown in Fig. 5(c), the density profiles of Ne and C were similar to that of the electrons. Therefore, accumulation was not significant for Ne and C. Since there is no source for Ne in the main plasma, the continuity

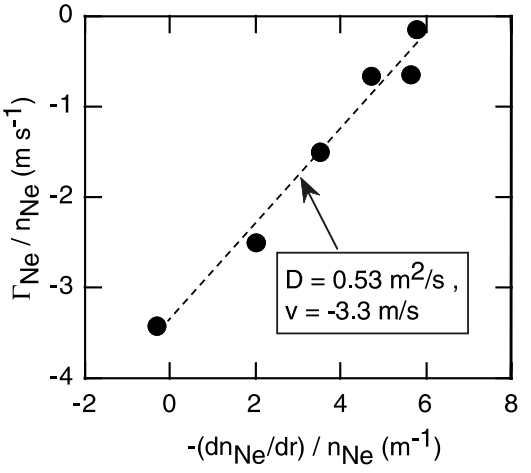

Fig. 6. Plot of Γ_{Ne}/n_{Ne} as a function of $-(dn_{Ne}/dr)/n_{Ne}$ at the ITB (at $r = 0.54$ a) at 5.6–6.3 s in the discharge shown in Fig. 2. A fitted line is also shown.

equation for Ne can be expressed using a diffusion coefficient D and inward velocity v as follows:

$$\Gamma_I/n_I = -D(dn_I/dr)/n_I + v, \quad (1)$$

where Γ_I and n_I are the flux and density of impurity I, respectively. Fig. 6 shows a plot of Γ_{Ne}/n_{Ne} as a function of $-(dn_{Ne}/dr)/n_{Ne}$ at the ITB after Ne injection, where Γ_{Ne} was derived from the time evolution of the Ne density profile. The data can be fitted to a line on the assumption that $D = 0.53$ m^2/s and $v = -3.3$ m/s. By a neoclassical transport model [14] including collisions with C, the transport coefficients and profiles of Ne ions were calculated. The calculated diffusion coefficient and inward velocity were $\sim$0.1 and $\sim$−2 m/s at the ITB. Therefore, the experimentally derived inward velocity was almost consistent with the calculated one. However, the experimentally derived diffusion coefficient was larger than the calculated one. The ratio of the calculated Ne density inside the ITB to that outside the ITB was by two orders higher than the ratio of the electron density inside the ITB to that outside the ITB.

For study of Ar transport, soft X-ray emission profiles were measured in a reversed-shear hydrogen discharge. Fig. 7 shows the ion and electron temperature, electron density, and normalized soft X-ray emission. ITBs were clearly observed in the profiles of the ion and electron temperature and electron density. The ratio of the electron density inside the ITB to that outside the ITB was about 3. As shown in Fig. 7(b), the measured soft X-ray emission profile could not be explained on the assumption that the Ar density profile was similar to the electron density profile. The soft X-ray profile could be explained on the assumption that the ratio of the Ar density inside the ITB to that outside the ITB was six times higher than the ratio of the electron density inside

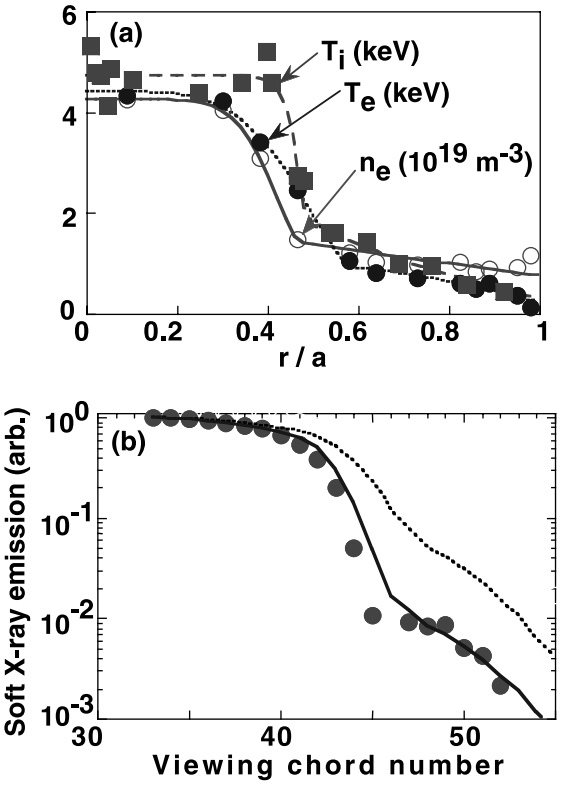

Fig. 7. (a) Ion and electron temperature, electron density, and (b) normalized soft X-ray emission (the solid circles are the measurement, the broken line is the calculation on the assumption that the Ar density profile is similar to the electron density profile, and the solid line is the calculation on the assumption that the ratio of the Ar density inside the ITB to that outside the ITB was six times higher than the ratio of the electron density inside the ITB to that outside the ITB) in a hydrogen discharge with Ar injection. The viewing chords of the soft X-ray emission measurement and the plasma configuration are shown in Fig. 1.

the ITB to that outside the ITB. Thus, accumulation was significant for Ar. Compared with results for C and Ne, it is suggested that accumulation is larger for more highly charged impurities. Similar results have been obtained in JET reversed-shear discharges [8]. This tendency is qualitatively in agreement with neoclassical transport theory. However, the accumulation observed for Ar in the present study was much smaller than that predicted by the neoclassical transport theory, since the theory predicted that the Ar density inside the ITB was by many orders higher than that outside the ITB.

The Ne X line intensity rolled over around 6.4 s in Fig. 2. However, the time constant of the intensity decrease was long. The Ne density could not be controlled by pumping, and most of the Ne recycled. Further enhancement of recycling in the divertor was required to increase the pumping efficiency and control the Ne density.

4. Summary

Ne injection was effective for obtaining a high radiation loss power fraction with high confinement at high density in reversed shear plasmas. Even with divertor plasma detachment and an X-point MARFE, the improved confinement with the ITB was maintained. On the other hand, Ar injection resulted in excessive radiation loss enhancement inside the ITB. Accumulation was not significant for Ne and C, but was significant for Ar. These results suggest that accumulation is larger for more highly charged impurities, and this tendency is qualitatively in agreement with neoclassical transport theory. However, the accumulation observed in the present study was much smaller than the theoretical prediction. For Ne, while the inward velocity at the ITB was almost consistent with the neoclassical transport calculation, the diffusion coefficient was larger than the calculation. The effective confinement time for Ne was long, and further enhancement of recycling in the divertor was required to control the Ne density.

Acknowledgements

The authors are grateful to Dr W.A. Houlberg of Oak Ridge National Laboratory and Mr E. Matsumoto of CSK Corporation for development of an impurity transport code. They wish to express their gratitude to Dr R. Dux of Max-Planck-Institut für Plasmaphysik for providing atomic data.

References

[1] H. Kubo et al., Nucl. Fusion 41 (2001) 227.
[2] J. Ongena et al., Phys. Plasmas 8 (2001) 2188.
[3] H. Kubo and the JT-60 Team, Phys. Plasmas 9 (2002) 2127.
[4] K. Itami et al., Fusion Energy 1997, Proceedings of the 16th International Conference on Fusion Energy, Montreal, 1996, vol. 1, IAEA, Vienna, 1996, p. 385.
[5] P.C. Efthimion et al., Nucl. Fusion 39 (1999) 1905.
[6] H. Takenaga and the JT-60 Team, Phys. Plasmas 8 (2001) 2217.
[7] H. Chen et al., Nucl. Fusion 41 (2001) 31.
[8] R. Dux et al., Proceedings of the 28th EPS Conference on Controlled Fusion and Plasma Physics, Funchal, vol. 25A, European Physical Society, Mulhouse, 2001, p. 505.
[9] P.N. Yushimanov et al., Nucl. Fusion 30 (1990) 1999.
[10] T. Fujita et al., Phys. Rev. Lett. 87 (2001) 085001-1.
[11] S. Sakurai et al., J. Nucl. Mater. 290–293 (2001) 1002.
[12] N. Hosogane et al., Fusion Energy 1998, Proceedings of the 17th International Conference on Fusion Energy, Yokohama, 1998, vol. 3, IAEA, Vienna, 1999, p. 903.
[13] ITER Physics Expert Groups on Confinement and Transport and Confinement Modelling and Database, Nucl. Fusion 39 (1999) 2175.
[14] W.A. Houlberg et al., Phys. Plasmas 4 (1997) 3230.